Multifunctional Nanoparticles for Imaging Guided Interventions

Yousef Haik[1,2], Basel al-Ramadi[2], Bashar Issa[2], Shahnaz Qadri[1], Saleh Hayek[1], Hassan Hijaze[2]

[1]Center of Research Excellence in Nanobiosciences, University of North Carolina at Greensboro, NC
[2]United Arab Emirates University, Al Ain, UAE

We describe multifunctional magnetic nanoparticles (MNPs) encapsulated in thermosensitive, drug-bearing shells and delivered to the tumor site by genetically modified and non-pathogenic strains of bacteria with known affinity to tumors for an effective and minimally invasive protocol for tumor management. The magnetic nanoparticles also serve as a non-invasive imaging contrast agent, heating agent as well as thermometry monitoring agents. We have shown an efficient tumor management on a mouse model utilizing the MNPs. Our studies showed that these novel MNPs significantly reduce the progress of tumor and prolong the animal life and function as an imaging contrast to visually monitor the tumor treatment and evolution.

An ideal therapeutic approach is to target multiple facets of the cancerous process while sparing the normal cells; a cocktail of drugs may achieve this goal if it can be delivered to specific tumor target to achieve optimal drug levels in the tumor without increase it's systemic side effects. However, multiplexing the diagnosis, targeted delivery, and monitoring remains a major technical challenge for cancer research.

Hyperthermia is a known modality of cancer therapy based on the vulnerability of the tumor cells to high temperatures. The viability of the cancerous cells is reduced and their sensitivity to chemotherapy and radiation is increased by raising the temperature of the target tissue to 42- 46°C[1-5]. Cancer cells have high potential to be destroyed at about 43°C while normal cells can survive higher temperatures of 46°C. Various methods of applying hyperthermia has been tried, such as the use of hot water, capacitive heating, and inductive heating of malignant cells[6-9]. The possibility of treating cancer by artificially induced hyperthermia has lead to the development of many different devices designed to heat malignant cells while sparing surrounding healthy tissue[10-12].

A number of studies have demonstrated the therapeutic efficacy of hyperthermia form of treatment in animal models[5] but the application of this technology to human patients is just starting[13]. Experimental investigations of the application of magnetic materials for hyperthermia date back to 1957 when Gilchrist[14], heated various tissue samples using γ - Fe_2O_3 particles of 20-100 nm size exposed to a 1.2 MHz magnetic field. Since then, there have been numerous publications describing a variety of schemes using different types of magnetic materials, different field strengths and frequencies and different methods of encapsulation and delivery of the particles[15-24]. In broad terms, the procedure involves dispersing magnetic particles throughout the target tissue, and then applying an AC magnetic

field of appropriate strength and frequency to cause the particles to heat. This heat conducts into the immediately surrounding diseased tissue where cancerous cells are destroyed if the temperature can be maintained above the therapeutic threshold of 42°C for at least 30 min. Whereas the majority of hyperthermia devices are restricted in their utility because of unacceptable coincidental heating of the surrounding normal tissue, magnetic particle hyperthermia is appealing because it offers a way to ensure that only the intended target tissue is heated. The concept is based on the principle that a magnetic particle can generate heat by hysteresis loss (other forms of heat dissipation based on particle size and composition may apply) when placed in a high frequency ~1 MHz magnetic field[25]. It has been shown that malignant cells take up nine times more MNPs than normal cells[26]. Therefore the heat generated in malignant cells is more than that in normal cells. Also, as blood supply in the cancerous tissues is subnormal the heat dissipation is much slower. Hence, the temperature rise in the region of tumor is higher than in the surrounding normal tissues. It is therefore expected to have a stronger antitumoral effect in areas with more concentrated heat.

The latest magnetic hyperthermia modalities are based on micro- and nano-scale mediators in the form of an injectable colloidal dispersion of magnetic particles and may be performed according to three strategies: arterial immobilization hyperthermia - AEH, direct injection hyperthermia - DIH, and intracellular hyperthermia - IH[27]. All these three approaches lack the capacity to assess the loading and distribution of particles at the tumor site, continuous monitoring of the immobilization, and treatment progress. We report a novel procedure that provides image-guided hyperthermia for tumor treatment; this procedure uses novel classes of multifunctional magnetic nanoparticles and has been shown to be safe, durable, and have excellent heating ability.

Image-guided therapies provide a unique multimodal approach to overcome the challenges associated with non-invasive monitoring of the therapy. Nanotechnology may offer solutions in overcoming these challenges by providing smart materials with multifunctional abilities that are created by controlling their physical properties during the synthesis process. Magnetic particles have been used as contrast agents, therapeutic agents and drug delivery agents[28-31].

Procedures such as hyperthermia therapy, cardiac arrhythmias treatment and heat sensitive promoters in gene therapy require temperature change monitoring. MRI thermometry overcomes problems associated with invasive temperature monitoring techniques such as thermocouples and fiber optics. In the current MRI thermometry the temperature variation is detected by measuring small changes in the proton resonant frequency[32], longitudinal relaxation time[33] or apparent diffusion coefficient[34]. However, these techniques have low temperature sensitivity and influenced by the local motion and magnetic susceptibility variation[35]. Liposome-encapsulated gadolinium chelates that have phase change characteristic were reported[36]. The temperature during the phase transition can be indicative of the local tissue temperature. However, this technique provides a one value for the temperature not a map of temperature distribution and requires careful design for the carrier.

Material with detectable physical property at different temperatures provides a suitable alternative for thermo-mapping at different locations. Coupling, the temperature dependence with a physical quantity that can be measured non-invasively provides a unique

technique for temperature mapping in deep-seated tissue. Our MNPs have magnetic moment temperature dependence that can provide the desired multifunctional actions. They have a contrast ability signature, temperature signature, and can be utilized as agents for hyperthermia therapy. The difference in magnetic moment size between the tissue and the MNPs causes additional contrast in magnetic resonance imaging. MNPs with steep variation in their magnetic moment as a function of temperature elevation provide information about the tissue temperature.

We synthesized multifunctional nanoparticles in the form of $ZnGd_xFe_{(2-x)}O_4$. Various samples of Gd-substituted Zn Ferrite nanoparticles were synthesized using chemical co-precipitation method in which the metal salts (e.g., $FeCl_3$, Fe_2SO_4, $ZnSO_4$, $GdCl_3$) were added to an NaOH solution. After vigorous stirring and filtration, newly synthesized particles were washed and then allowed to air dry at room temperature[37].

When comparing the characterization data of the Gd-substituted Zn Ferrite particles with that of the Zn-Ferrite particles it was noticed that addition of Gd in small amounts lead to an increase in the Curie temperature (Tc) as well as the pyromagnetic co-efficient of the nanoparticles. Figure 1-a shows the magnetic moment of particles as a function of temperature for x=0.02, and Figure 1-b shows the variation of their Tc as a function of x. The XRD pattern is shown in Figure 2. The pattern confirms the formation of single-phase spinel structure. TEM micrograph of the dispersion of ZnGd-ferrite nanoparticles in ethanol deposited over a Cu grid are shown in Figure 3. The sample consists of a dispersion of almost spherical particles with a narrow size distribution. The histogram of the diameter from a statistical analysis over 100 particles is shown in the insert. The distribution fits a Gaussian distribution with mean±sd diameter of 5.5 ± 0.9 nm. The obtained value is closed to that obtained from XRD measurement indicating a high crystalline degree of all particles[38]. The nanoparticles systems developed generate sufficient heat (specific absorption rate SAR [W/g]) and stop heating at the measured Tc. The power dissipated from the nanoparticles systems was calculated from the area enclosed by the hysteresis loop. These chemically synthesized nanoparticles were tested for cyto-toxicity by MTT assay, on normal human and cancerous cell lines. No significant toxicity was found. No signs of toxicity were observed on 25 BalB/c mice according to http://ctep.info.nih.gov protocols.

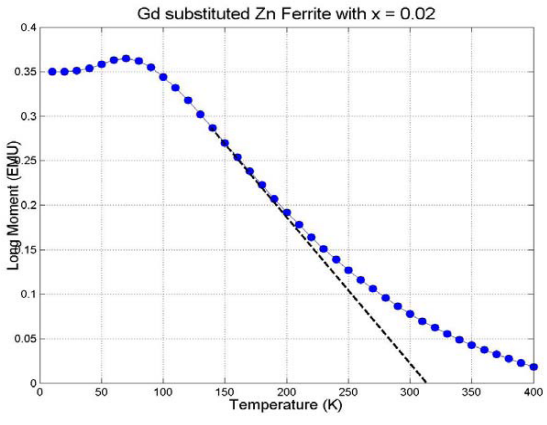

Figure 1-a. Temperature dependance of magnetization

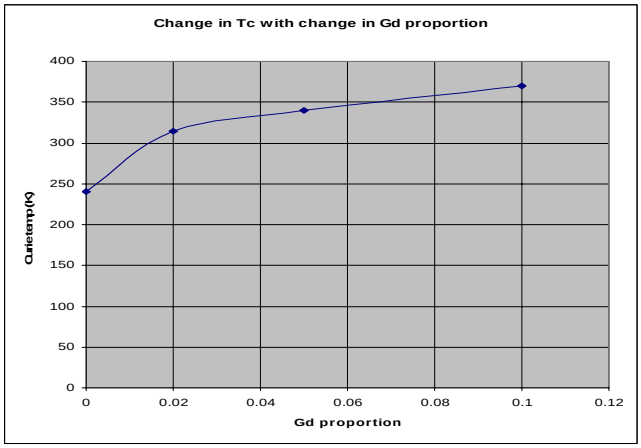

Figure1-b. Change in Tc as a function of Gd

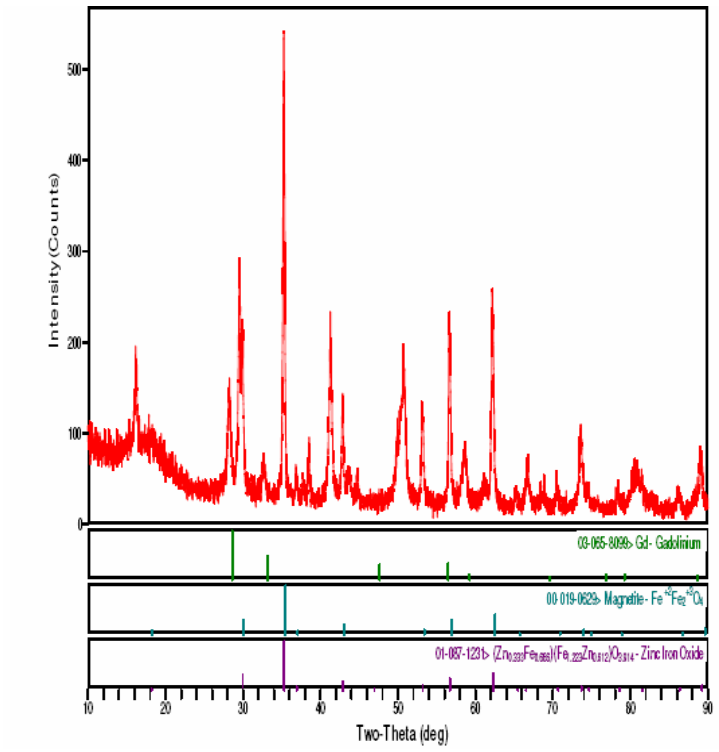

Figure2. X-ray diffraction pattern

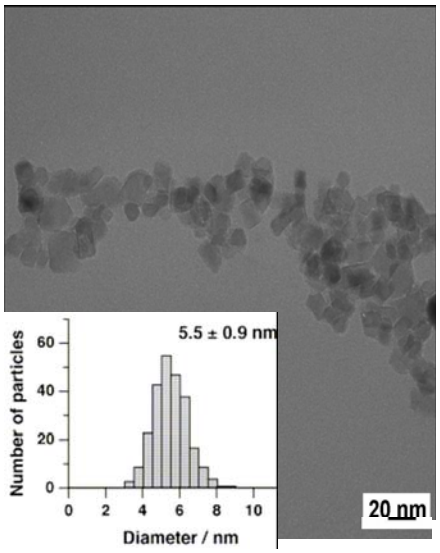

Figure 3 . TEM and particle size distribution

We further investigated the use of these MNPs, as new MRI contrast agents. We hypothesized that if relaxation rates are shown to be temperature-sensitive it is anticipated that these agents would then be used as thermometry agents and hence improve the efficacy of many clinical procedures, e.g. hyperthermia treatment.

We have investigated the MR longitudinal (T1) and transverse (T2) relaxation enhancement due to different concentrations of the Zn-Gd-Fe family of uncoated MNPs. A fast spin-echo (FSE) imaging sequence has been used at a field strength of 1.5 T with the following parameters: for the T1 measurement an inversion recovery sequence is used with TI = 50, 100, 300, 700, 1200, 2000, and 3000 ms; with a TE = 15 ms; while for the T2 measurement a spin-echo sequence with TE = 15, 30, 45, 60, 100, and 150 ms. Particles were prepared in viscous cellulose solutions to maintain them in suspension. The concentrations were C = 0.29, 0.57, 1.14, 2.28, and 03.40 mmol/kg weight in addition to the control (i.e. C = 0.0). Signal intensity is plotted versus TE for various concentrations (Figure 4) at 23 ^{o}C. Single exponential curve was fitted to the data using non-linear programming (Levenberg-Marquardt) minimizing an error function to yield the time constant T2. R2 enhancement is linear with C as shown in Figure 5. The relaxivity (r_2) as defined by the equation ($R_2(C) = R_{20} + r_2 C$) is 240 (s mmol/kg)$^{-1}$. R_{20} is the transverse relaxation rate in the absence of MNPs. Similar analysis for the T1 data revealed $r_1 = 1.8$ (s mmol/kg)$^{-1}$.

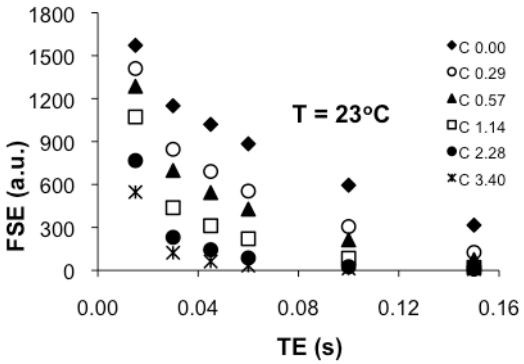

Figure 4. FSE signal variation with echo-time

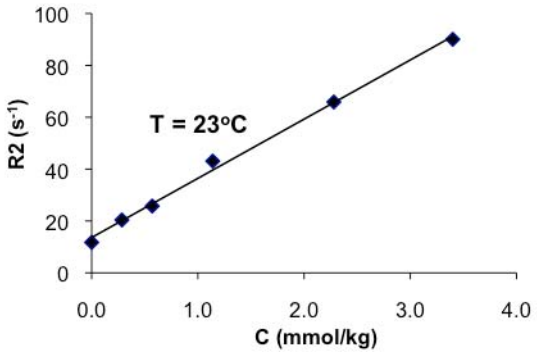

Figure 5. Transverse relaxation rate vs. concentration at temperature = 23°C.

Spin-echo T2 weighted for different values of the echo time (TE). Signal decay variation with both concentration (different tubes) and TE is clearly demonstrated. The calculated values for the relaxation rates R1 and R2 are shown in Table 1 along with their ratio R2/R1 at 23 °C. As expected for superparamagnetic particles R2 >> R1. The effect of MNPs will be to produce negative image contrast (i.e. signal reduction due to T2 wieghting is more pronounced than signal elevation due to T1 weighting).

Table 1: R1 and R2 values at different concentrations of the nanoparticles at 23 °C.

C (mmol/kg)	**R1 (s^{-1})**	**R2 (s^{-1})**	**R2/R1**
C 0.0	0.64	11.7	18.3
C 0.025	0.68	20.4	29.9
C 0.050	0.72	25.8	36.0
C 0.100	0.82	43.1	52.4
C 0.200	0.98	65.9	67.1
C 0.300	1.11	90.0	81.5

Upon heating the samples to temperatures blow and above the particles Curie temperature (42.8°C) the R1 and R2 are measured for the different concentrations. Normalized values of R1 and R2 are plotted in Figure 6 and 7 respectively where it is shown that both relaxation rates increase lineraly with both concentration of the MNPs and temperature.

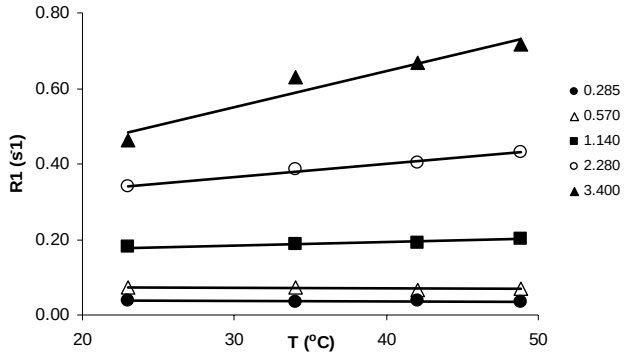

Figure 6 The linear variation of 1/T1 (normalized) with temperature increases with the concentration of MNPs.

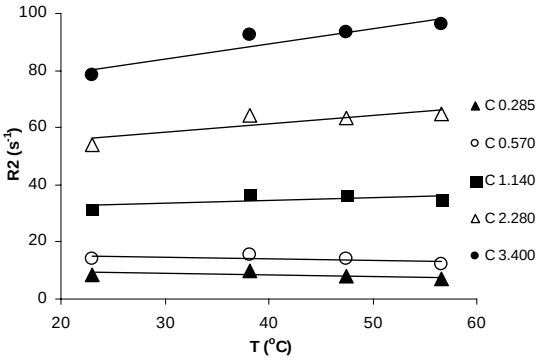

Figure 7. As for 1/T1 the variation of 1/T2 (normalized) is linear with temperature, however, the slopes are larger.

The relaxivity (r_2) values (in kg s^{-1} $mmol^{-1}$) are summarized in Table 2. Relaxivity increases linearly with temperature and data has a positive slope 0.173 and R-squared value 0.92.

Table 2: r_2 values at different temperatures

T (°C)	r_1 (kg s^{-1} $mmol^{-1}$)	T (°C)	r_2(kg s^{-1} $mmol^{-1}$)
23.0	0.140	**23.0**	22.8
34.4	0.186	**38.2**	27.1
43.0	0.197	**47.4**	27.6
48.9	0.212	**56.6**	28.8

MR relaxation enhancement is demonstrated with new class of magnetic nanoparticles that have already been used for hyperthermia applications. The contrast ability (in particular R2) is found to vary linearly and significantly with concentration. Furthermore, the relaxation enhancement of these new contrast agents exhibits linear variation with temperature. This would allow the use of these MNPs particles, in addition to their role as contrast agents, in temperature monitoring and hyperthermia applications.

The use of non-pathogenic bacteria in cancer therapy is an innovative approach that stemmed from the observation that some bacteria have tropism for tumors where they replicate and accumulate reaching concentrations exceeding 1000-fold their concentration in other target organs. It has been also shown that attenuated *Salmonella typhimurium* strains accumulate at tumor sites when injected in tumor-bearing mice while rapidly clearing from

the blood of normal mice[39-44]. Because of their selectivity for tumor tissue, these bacteria would make ideal carriers for contrast agents. The use of attenuated bacteria strains as carriers for gene vectors[45], vaccines[46] and chemotherapeutic agents[47] has been reported. However, there is limited information on the ability of loading bacteria with MNPs.

We used bacterial delivery system to convey the NMPs alone or together with other cancer drugs to the tumor site. Experiments were conducted to evaluate the upload of MNPs into the bacteria membrane. *Salmonella* BR 509 was used. These bacteria are rod shaped with 1 micron in length. Ultrafine particles were incubated with *Salmonella*. Figure 8 shows SEM micrographs of the MNP-bacteria. It was observed that small size particles were diffused into the cell membrane. We were able to separate the MNP-bacteria from the sample using a permanent magnet.

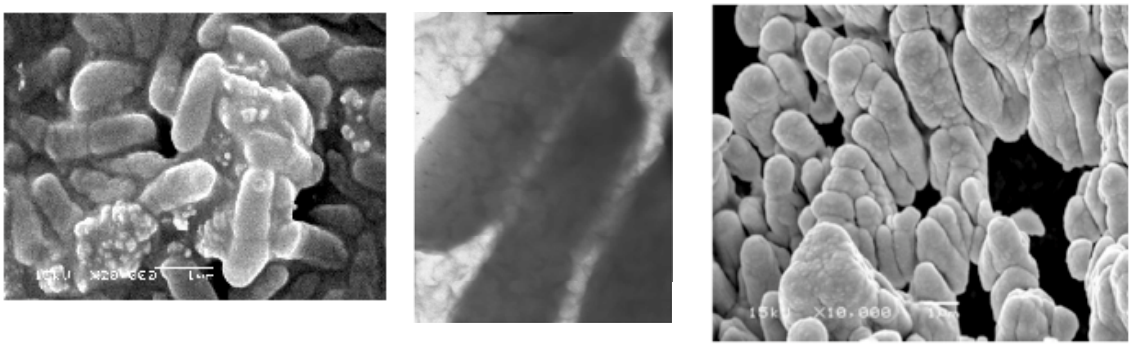

(a) (b) (c)

Figure 8 (a) SEM of encapsulated MNPs attached on the cell membrane of *Salmonella,* (b) shows that smaller NMPs entered the *Salmonella's* membrane and (c) shows vertically aligned Salmonella when exposed to a magnetic field placed on top of the slides.

We demonstrated the intake of MNP in a strain of attenuated *Salmonella typhimurium* BRD509. The targeting of drug-coated MNP-loaded *Salmonella* organisms to tumor sites have a great advantage over systemic administration of the anti-cancer drug as it would significantly reduce the toxicity associated with prolonged treatment with high doses of chemotherapeutic drugs. In here we encapsulated the MNPs along with anti-tumor drug (5FU or doxirobucine) in a thermosensitive shell. *Salmonella* organisms carried the coated shells to tumor tissue. Under the influence of a magnetic field at 0.963MHz, the tumor-targeted MNP generate heat up to 42° to 43°C, thus releasing the drug specifically at the tumor site. This way, non-specific exposure of the host to the chemotherapeutic agent is avoided.

The conditions for uptake of MNPs by live *Salmonella* bacteria were optimized. In these experiments, 1 x 10^8 colony forming units (CFUs) of *Salmonella* strain BRD509 were incubated with MNPs in saline buffer. At the end of the incubation period, the bacterial suspension was spun down and the supernatant was aspirated. After resuspending the bacterial pellet in 1 ml saline, the bacterial suspension was subjected to a 0.45 Tesla permanent magnet for 15 minutes on the outside surface of the eppendorf tube. The remaining supernatant, presumably containing non-MNP-associated bacteria, was aspirated, and replaced with fresh saline. This procedure was repeated 3 times in total. Aliquots were removed from the bacterial suspension before and after each wash cycle and plated to determine the actual count of bacterial CFUs. Using this procedure, the number of bacterial CFUs remaining after four cycles of magnetic separation and washing (which most likely represents the number of bacteria actually associated with MNPs) was determined, and hence the % of bacteria associated with MNPs was calculated. Figure 8 illustrates the loss of non-MNP-associated *Salmonella* organisms, following co-incubation with MNPs at 24ºC for 120 minutes, after each cycle of wash. It demonstrates that all bacteria not associated with nanoparticles are effectively removed by the 3rd wash cycle. Furthermore, varying the incubation conditions have a clear impact on the uptake of MNPs by the bacteria. Incubation of MNPs with live *Salmonella* organisms at room temperature resulted in the most optimal uptake, which was about 6% (*$6x10^6$, sufficient for the loading purpose*). The fact that the association appears to be strong suggests that it is feasible to use the MNP-loaded, or MNP-associated, *Salmonella* organisms in tumor targeting in vivo.

B6 mice (20g ± 3g) were housed in appropriate isolated caging with sterile rodent laboratory chow and acidified water *ad libitum* and a 12-h light/dark cycle. B6 mice were implanted subcutaneous in the mid of tail by 50 micro liter volume of PBS with approx. 300,000 melanoma cells, 99% viability. Tumor was visible after 20 days, 1-2mm diameter. Four groups of five each were prepared such that one group with no treatment (control), second group with drug therapy (5FU) only, third group with hyperthermia only and the fourth group with integrated particle that has the drug and heating agent encapsulated in the thermosensitive polymer. The treatment started after a month from inoculation of the cells. In this experiment control group was given saline, hyperthermia (nanoparticles alone) group received nanoparticles in a concentration of 20mg/kg of body weight and followed by hyperthermia at 0.963MHz for 45 minutes. Six doses were given after every two days gap. Tumor volume was measured every two days until survival of mice. Tumor volume corresponds to width² X length / 2. Tumor temperature rises till 42-43ºC, and was monitored during the experiment. Figure 9 shows the temperature distribution immediately following non-invasive magnetic heating of shells carrying drug load and MNPs and injected ip into the tail of the treated mouse.

Close up pictures were taken for tumor to present significant difference. It was noticed that blood flow to tumor was increased due to increase in temperature. The survival measurements showed that hyperthermia treated mice with encapsulated drug have survived the longest (5 times more than drug alone treated mice) a subsequent measurement of controlled tumor growth.

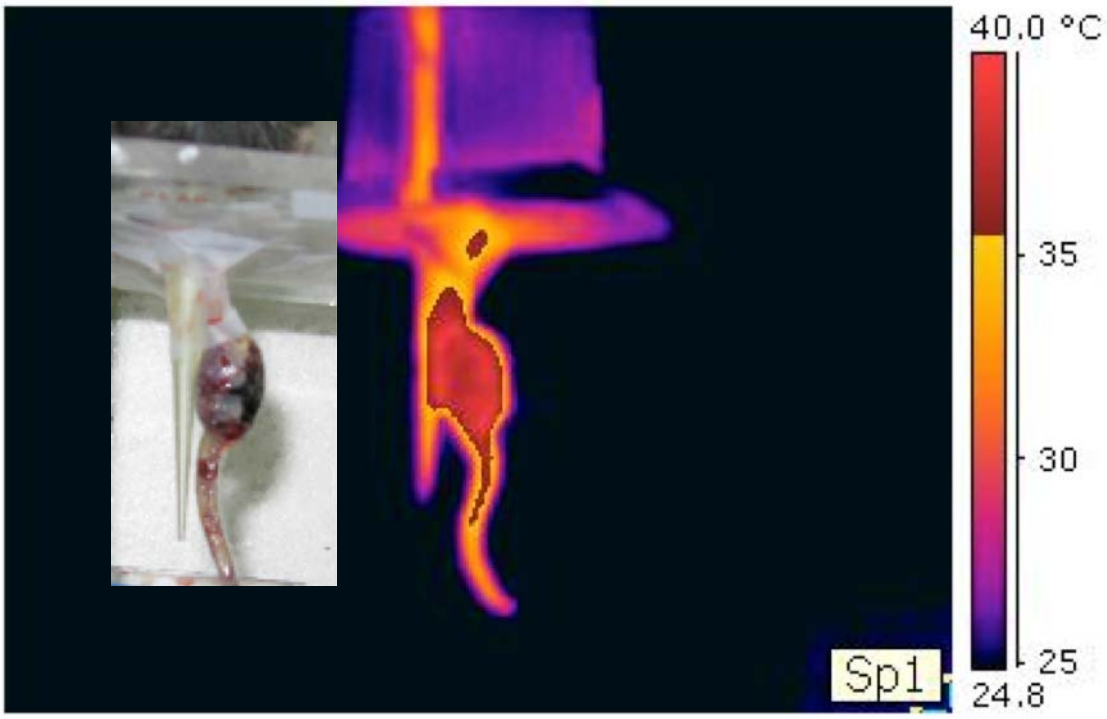

Figure 9 Temperature map of heated tumor containing MNPs. The inner pictures show the tumor just before introducing the treatment.

Figure 10 shows the measured tumor volume as a function of time for all groups post treatment. It is clearly shown that the multifunctional therapy has better efficacy than each of the therapies if they administered alone. Figure 11 shows the survival curve for all groups. It is clear that the volume of the tumor has reduced dramatically and the animals survived the most when the hyperthermia therapy was implemented.

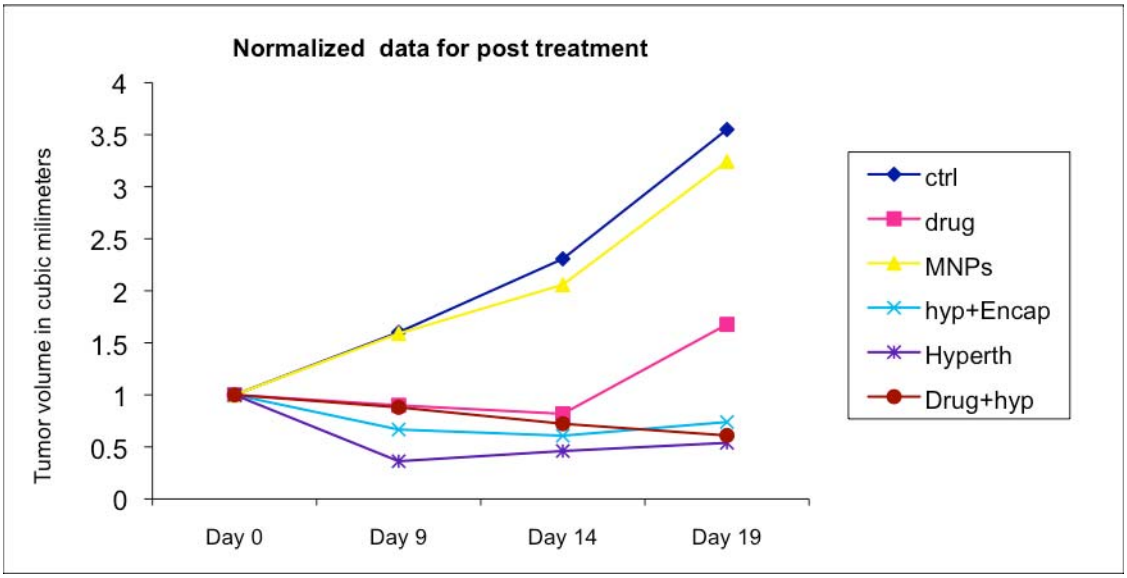

Figure 10. Tumor volumes for all groups. The tumor volume is normalized with the control starting the first day of treatment. Day 0 is day when treatment started and the 30th day after the inoculations of the tumor

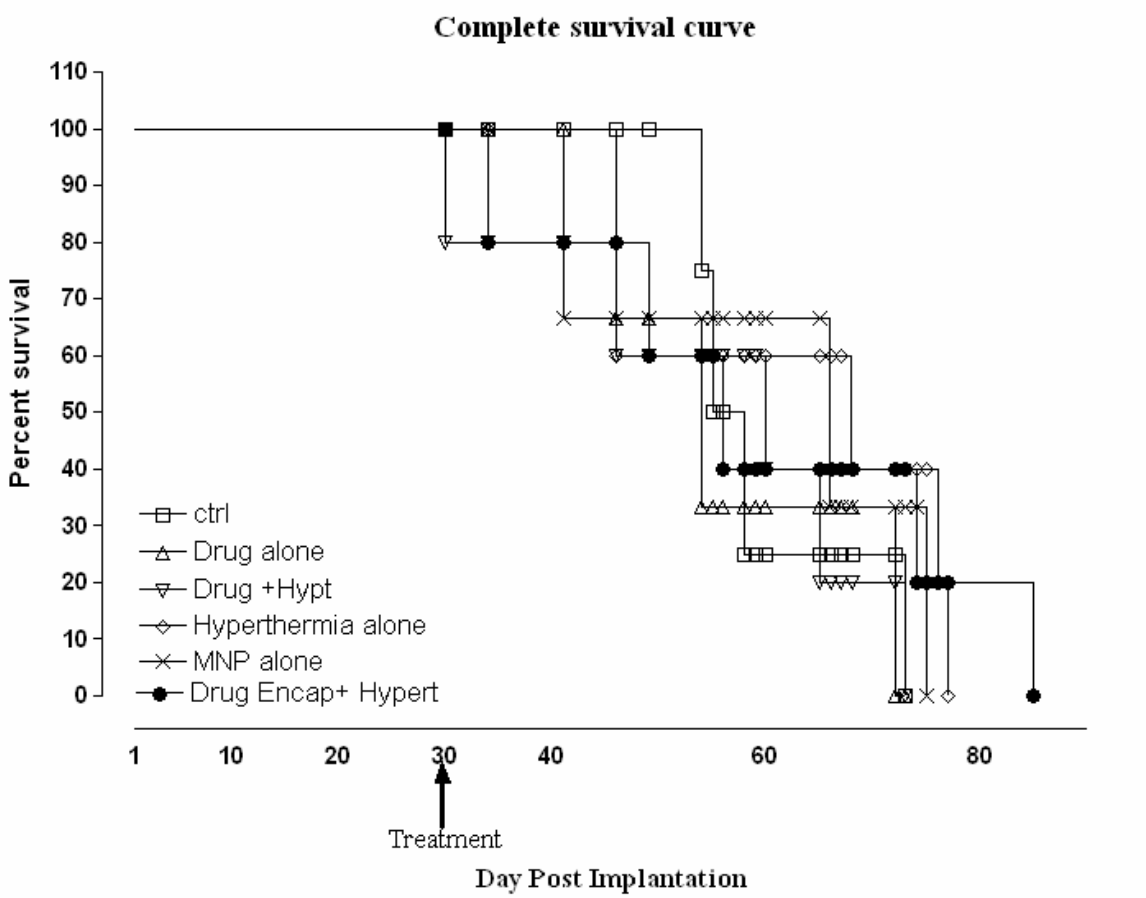

Figure 11. Survival of the animals of all groups.

We have also tested the ability of bacteria to deliver the load of drugs without having to heat the tumor. Figures 12 and 13 demonstrates that when hyperthermia is utilized the effectiveness of delivery and treatment are more when hyperthermia is utilized.

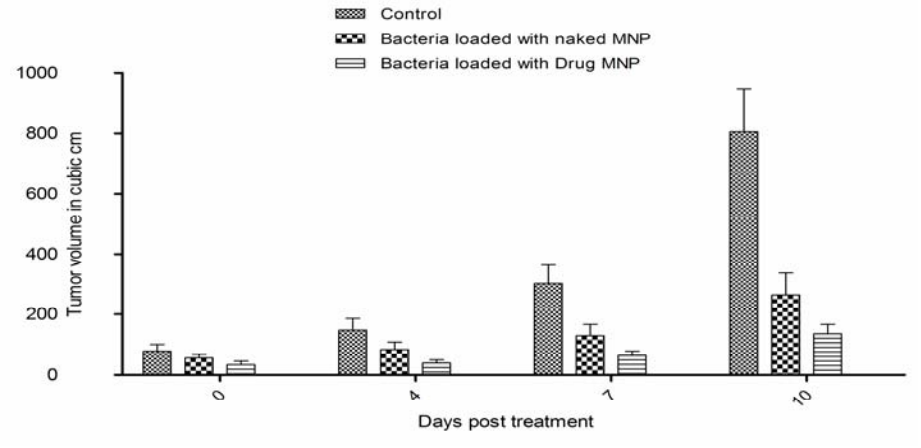

Figure 12. Tumor volume post treatment of control, bacterial loaded with MNPs (no drug) and bacteria loaded with shelled drug and MNP. Bacterial delivery is effective. The mechanism of drug unloading is not fully understood, but may be associated with the bacteria cellular division at the tumor.

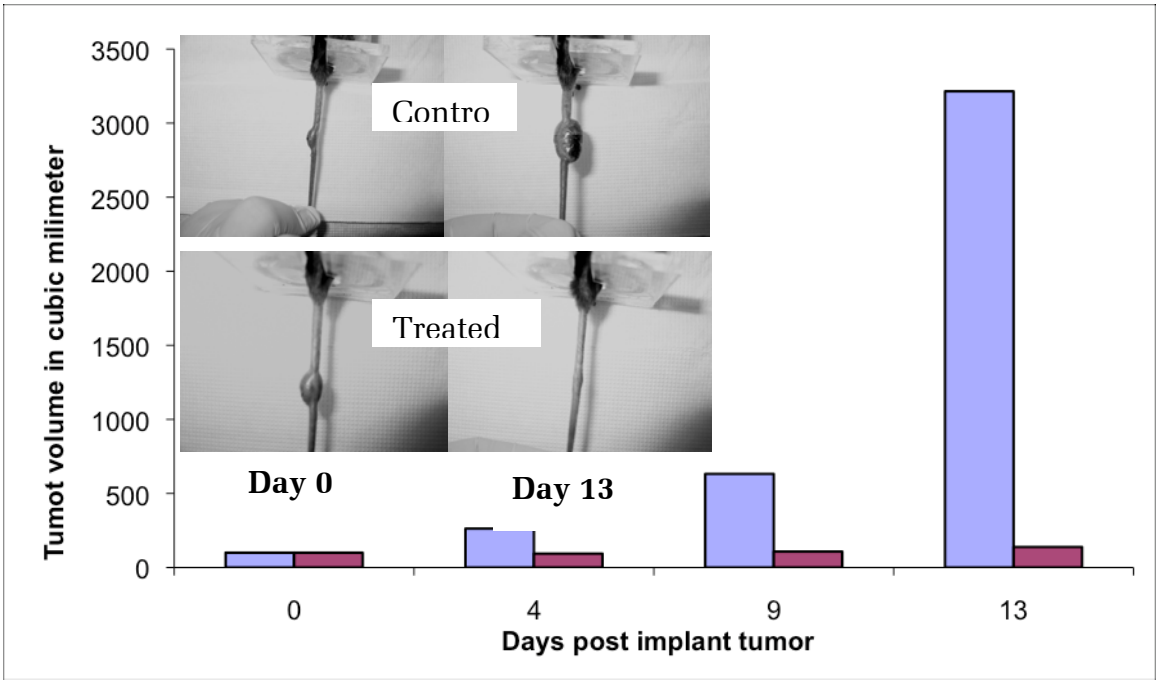

Figure 13 shows the normalized tumor volume for control and treated groups. Drug and MNPs were loaded in a thermosensitive shell loaded on a bacteria carrier. The picture in the middle of the bar chart shows the change in tumor volume for a sample of control and treated mice.

In conclusion we demonstrated the functionalization of a potential imaging guided intervention that employs multifunctional magnetic nanoparticles with potential to provide targeted drug delivery and non-invasive monitoring of drug localization and thermometry. A smart drug carrier with high affinity to tumors is utilized to site-specific delivery of thermosensitive shells bearing anticancer drug and nanoparticles. Non-invasive localized heating is induced by a remote alternating magnetic field. The intervention when applied to induced tumors showed preferred therapeutic management of the tumor.

Acknowledgements

This project was partially supported by the University of North Carolina at Greensboro and the United Arab Emirates University Research Offices.

1. Shinkai, M., J. Biosci. Bioeng., 94 (6), pp. 606, 2000.
2. Mitsumori, M., Hiraoka, M., Shibata, T., Okuno, Y., Nagata, Y., Nishimura, Y.,Abe, M., Hasegawa, M., Nagae, H., and Ebisawa, Y., Hepato-Gastroenterology, 43, pp. 1431–7, 1996
3. Minamimura, T., Sato, H., Kasaoka, S., Saito, T., Ishizawa, S., Takemori, S.,Tazawa, K., and Tsukada, K., Int. J. Oncol., 16, pp. 1153–8, 2000.

4. Hilger, I., Fruhauf, K.,Andra, W., Hiergeist, R., Hergt, R., and Kaiser, W. A., Acad. Radiol., 9 , pp. 198–202, 2002
5. Moroz, P., Jones, S. K., Gray, B. N., Int. J. Hyperthermia, 18(4), pp. 267–284, 2002.
6. Cavalier, R., Ciocatto, E. C., Giovanel, B., Heidelbe, C., Johnson, R. O., Margotti,M., Mondovi, B., Moricca, G., Rossifan, A., Cancer, 20(9), pp.1351, 1967
7. Stauffer, P. R., Cetas, T. C., Fletcher, A. M., Deyoung, D. W., Dewhirst, M. W.,Oleson, J. R., Roemer, R. B., IEEE Trans. Biomed. Eng., 31(1), pp.76-90, 1984.
8. Lin, J. C., Wang, Y. J., 1987, Int. J. Hyperthermia, 3(1), pp. 37-47, 1987.
9. Ikeda, N., Hayashida, O., Kameda, H., Ito, H., Matsuda, T., Int. J. Hyperthermia, 10(4), pp. 553-561, 1994.
10. Wust, P., Hildebrandt, B., Sreenivasa, G., Rau, B., Gellermann, J., Riess, H., Felix, R.and Schlag, P. M., LancetOncol., 3, pp. 487-97, 2002.
11. Van der Zee, J., Ann. Oncol., 13, pp. 1173-84, 2000.
12. Moroz P, Jones S K and Gray B N J. Surg. Oncol. 77 259–69, 2001
13. Jordan, A., Scholz, R., Maier-Hauff, K., Johannsen, M., Wust, P., Nadobny, J.,Schirra, H., Schmidt, H., Deger, S., Loening, S., Lanksch, W., Felix, R., J. Magnet. Magn. Mater., 225(1–2), pp. 118-126, 2001.
14. Gilchrist, R. K., Medal, R., Shorey, W. D., Hanselman, R. C., Parrott, J. C. andTaylor, C. B., 1957, "Ann. Surg.,146, pp. 596–606, 1957.
15. Mosso, J. A., and Rand, R. W., Ann. Surg., pp. 663–8, 1972.
16. Rand, R. W., Snyder, M., Elliott, D. G., and Snow, H. D., Bull. Los Angeles Neurol. Soc., 41, pp. 154–9, 1976.
17. Gordon, R. T., Hines, J. R., and Gordon, D., Med. Hypotheses, 5, pp. 83–102, 1979.
18. Rand, R. W., Snow, H. D., Elliott, D. G., and Snyder, M., Appl. Biochem. Biotechnol., 6, pp. 265–72, 1981.
19. Borrelli, N. F., Luderer, A. A., and Panzarino, J. N., Phys. Med. Biol., 29, pp. 487–94, 1984.
20. Hase, M., Sako, M., and Hirota, S., Nippon-Igaku-Hoshasen-Gakkai-Zasshi, 50, pp. 1402–14, 1990.
21. Suzuki, S., Arai, K., Koike, T., and Oguchi, K., J. Japan. Soc. Cancer Therapy, 25, pp. 2649–58, 1990.
22. Chan, D. C. F., Kirpotin, D. B., and Bunn, P. A. Jr., J. Magn. Magn. Mater., 122, pp. 374–8, 1993
23. Jordan, A., Scholz, R., Wust, P., Fahling, H., Krause, J., Wlodarczyk, W., Sander,B., Vogl, T., and Felix, R., 1997, in vivo Int. J. Hyperthermia, 13, pp. 587–605, 1997.
24. Jordan, A., Scholz, R., Wust, P., Fahling, H., and Felix, R., J. Magn. Magn. Mater., 201, pp. 413–19, 1999.
25. Stauffer, P. R., Cetas, T. C., Fletcher, A. M., Deyoung, D. W., Dewhirst, M. W.,Oleson, J. R., Roemer, R. B., IEEE Trans. Biomed. Eng., 31(1), pp.76-90, 1984.

26. Xu X. J., Chew C. H., Siow K. S., Wong M. K., Gan L. M., Langmuir 15:8067, 1999
27. Hilger, I., Fruhauf, K.,Andra, W., Hiergeist, R., Hergt, R., and Kaiser, W. A., Acad. Radiol., 9 , pp. 198–202, 2002
28. Haik, Y., Chen C-J., US Patent Application 20050249817, 2005
29. Bettge, M., Chatterjee, J., Haik, Y., J Biomag. Res Tech 2(4), 2004.
30. Chatterjee, J., Bettge, M., Haik, Y., Chen C-J., J Mag MagMat 293:303-309, 2005
31. Sharma R., Haik Y., Chen C-J, J ExperNanoscience, 2(1):127-138, 2007
32. Ishihara Y, Calderon A, Watanabe H, Okamoto K, Suzuki Y, Kuroda K, Suzuki Y. Magn Reson Med 34:814–823, 1995.
33. Parker DL. IEEE Trans Biomed Eng 31:161–167, 1984.
34. Le Bihan D, Delannoy J, Levin RL. Radiology 171:853–857, 1989.
35. Rieke V, Pauly KB. J Magn Reson Imaging 27:376–390, 2008.
36. Chen, C-J., Haik, Y., Chatterjee, J., in Recent Research Developments in Magnetism and Magnetic Materials, Transworld Research Network, Recent ResearchDevelopment in Magnetism and Magnetic Materials, 1, 2003.
37. Chen, C-J., Hayek S., Mohite V., Yuan H, Chatterjee J., Haik Y. Chapter 11, in Cancer Nanotechnology-Nanomaterials for Cancer Diagnosis and Therapy, Edited by Nalwa H. S. and Webster T., 2006
38. Jain, R. K., N. S. Forbes N S., Proc NatlAcadSci USA. 98: 14748-14750, 2001
39. Al-Ramadi, B. K., Mol. Immunol. 38: 931-940, 2002
40. Al-Ramadi, B. K., Mol. Immunol. 39: 763-770, 2003
41. Al-Ramadi, B. K., Mol. Immunol. 40: 671-679, 2004
42. Al-Ramadi, B. K., Microbes Infect. 6: 350-359, 2004
43. Clairmont C., Lee K. C., Pike J., Ittensohn M., Low K. B., Pawelek J., Bermudes D., Brecher M., Margitich D., Turnier J., Li Z., Luo X., King I., Zheng L. M., J InfecDis, 181:1996-2002, 2000.
44. Bermudes D., Zheng L. M., King I C. 5(2):194-1999, 2002.
45. Jia L-J., Wei D-P., Sun Q-M., Jin G-H., Li S-F., Haung Y., Hua Z-C., Inter J Cancer, 2007.
46. Pawelek J M, Low K B, Dermudes D, Cancer Res, 20:4537-4544, 1997
47. Reisfeld R A, Niethammer A G, Luo Y, Xiang R., Immun Rev, 199:181-190, 2004